Hydrogen Production by Ethanol Reforming on Supported Ni−Cu Catalysts

Qihai Liu, Hongjun Zhou,* and Zhenyu Jia*

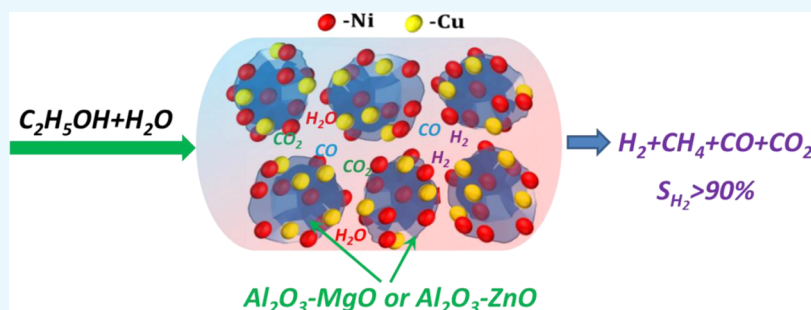Read Online

ACCESS | Metrics & More | Article Recommendations


ABSTRACT: Supported bimetallic Ni−Cu catalysts with different Ni−Cu loadings on alumina (Al_2O_3), alumina−silica (Al_2O_3−SiO_2), alumina−magnesia (Al_2O_3−MgO), alumina−zinc oxide (Al_2O_3−ZnO), and alumina−lanthanum oxide (Al_2O_3−La_2O_3) were prepared and tested in ethanol steam reforming for the production of hydrogen (H_2). These catalysts were characterized by X-ray diffraction, H_2-temperature-programmed reduction, ammonia-temperature-programmed desorption, X-ray photoelectron spectroscopy, thermogravimetry, and differential scanning calorimetry. Cu addition improved the reducibility of NiO. Among the as-prepared catalysts, $30Ni5Cu/Al_2O_3$−MgO and $30Ni5Cu/Al_2O_3$−ZnO demonstrated much higher H_2 selectivity and excellent coke resistance compared to the other investigated catalysts. Over $30Ni5Cu/Al_2O_3$−MgO and $30Ni5Cu/Al_2O_3$−ZnO, the respective H_2 selectivity was 73.3 and 63.6% at 450 °C and increased to 94.0 and 95.2% at 600 °C. The strong interaction of Ni−Cu and Al_2O_3−ZnO (or Al_2O_3−MgO) led to the formation of smaller and highly dispersed CuO and NiO species on the carrier, which is conducive to improved catalytic performance. These Al_2O_3−MgO- and Al_2O_3−ZnO-supported bimetallic Ni−Cu materials can be promising catalysts for hydrogen production from ethanol steam reforming.

1. INTRODUCTION

The synthesis and use of hydrogen has received considerable attention due to carbon pollution from conventional fuels. Of special interest is ethanol obtained by fermentation of renewable substances, considering the reproducibility of biomass feedstocks, good processability of liquid ethanol, and high hydrogen conversion.[1−3] Ethanol can be efficiently converted to the main product hydrogen (H_2) by the following reaction[4−6]

$$CH_3CH_2OH + 3H_2O$$
$$\rightarrow 6H_2 + 2CO_2, \Delta H^0_{298}$$
$$= +347.4 \text{ kJ/mol}$$
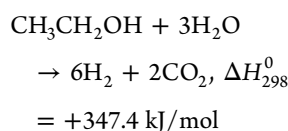
The thermodynamic ethanol reforming reaction usually consists of several reactions, starting with a dehydrogenation or dehydration reaction. The dehydrogenation reaction produces acetaldehyde, which is transformed into carbon monoxide and methane by C−C bond cleavage. However, carbon deposition in the process of producing ethylene from ethanol is an urgent problem to be solved. Generated CH_4 can form H_2 and CO via steam reforming, and a water−gas shift (WGS) reaction can convert CO to carbon dioxide (CO_2).

In general, transition metals such as Ni, Co, Pt, Pd, and Rh are often used to catalyze the production of hydrogen from ethanol due to their good activity and selectivity.[7−9] Ni is widely used as a catalyst thanks to its high activity in C−C bond cleavage, however, its use is limited by various disadvantages.[10−12] The reactivity of Cu is limited for hydrogen production from ethanol but good for dehydrogenation[13−15] and the WGS reaction. In addition, mixing in Ni and Cu can reduce CO production and improve coking

resistance for hydrogen production in ethanol using silica (SiO_2) as a carrier.

Among oxide carriers, alumina (Al_2O_3) carriers have excellent physical and chemical stabilities and are commonly used as catalysts for hydrogen production from ethanol.[16,17] However, the deactivation of Al_2O_3 due to carbon deposition greatly reduces its catalytic activity. To address these shortcomings, the researchers developed alkaline additives that readily adsorb water and improve the surface mobility of hydroxyl (OH) groups. Magnesium oxide (MgO) and solid solution magnesium oxide ($MgAl_2O_4$) have been developed and used to avoid coking on nickel-based carriers because they allow better dispersion of nickel powders.[18,19] Zinc oxide (ZnO) has basic characteristics as well as redox properties that accelerate the dehydrogenation of ethanol to acetaldehyde,[20] which is also promoted by lanthanum oxide (La_2O_3) and other lanthanide oxides. In addition, it was reported that SiO_2-stabilized Al_2O_3 used as the support for Pd catalysts can make the methane combustion more complete and employing $SiO_2–Al_2O_3$ as the support can slow down coking in the process of olefin hydrogenation.[21] Although many metal catalysts have been studied for hydrogen production from ethanol, further intensive investigations are required to explore efficient catalysts with high coke resistance and selectivity in the production of H_2.

To determine the effect of Cu and supports on the performance of bimetallic Ni−Cu catalysts in ethanol steam reforming, several metal-oxide-modified supports with varying Cu contents were investigated in this study. The composite supports $Al_2O_3–SiO_2$, $Al_2O_3–MgO$, $Al_2O_3–ZnO$, and $Al_2O_3–La_2O_3$ were prepared and used as bimetallic Ni−Cu catalyst supports. The catalysts were characterized by X-ray diffraction (XRD), H_2-temperature-programmed reduction (H_2-TPR), ammonia-temperature-programmed desorption (NH_3-TPD), X-ray photoelectron spectroscopy (XPS), thermogravimetric analysis (TGA), and differential scanning calorimetry (DSC). The results showed that $Al_2O_3–MgO$- and $Al_2O_3–ZnO$-supported Ni−Cu catalysts possessed much better catalytic performance than the other investigated catalysts.

2. RESULTS AND DISCUSSION

2.1. X-ray Diffraction Analysis. XRD patterns of the calcined 30Ni5Cu catalysts with different supports are shown in Figure 1. The major peaks at 2θ = 36, 46, and 67° are attributed to γ-Al_2O_3, and the peaks around 2θ = 18 and 60° are attributed to NiO species. The diffraction peaks of NiO and CuO are not observed in patterns (c) and (d), indicating that NiO and CuO might be well dispersed on the support. To further explore the relationship between the active species and the carrier structure, H_2-TPR experiments were conducted.

2.2. H_2-Temperature-Programmed Reduction. The H_2-TPR profiles of the catalysts are shown in Figure 2. Except for the 30Ni5Cu/Al_2O_3–La_2O_3 catalyst, the reduction curves of the catalysts generally contained two peaks. The low-temperature peak could be attributed to the reduction of dispersed small metal particle species (NiO or Ni−Cu mixed metal oxides), and the high-temperature peak probably resulted from the reduction of agglomerated coarse metal particle species.[22] The two reduction peak intensities of the 30Ni5Cu/Al_2O_3 catalyst were similar, and it was assumed that the amounts of dispersed fine metal and agglomerated coarse metal particle species were roughly the same. For 30Ni5Cu/Al_2O_3–SiO_2, the intensity of the high-temperature reduction
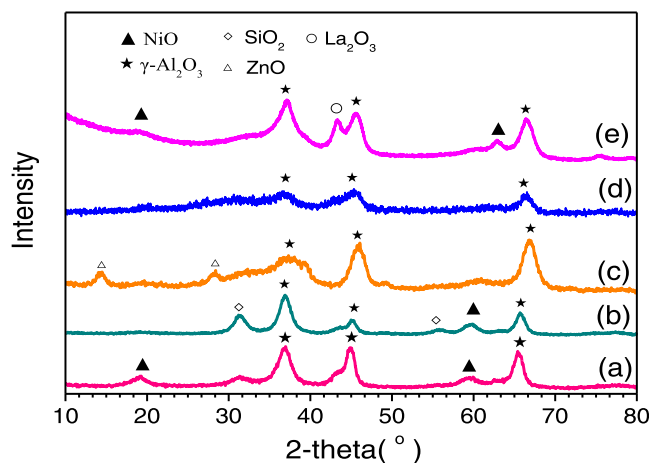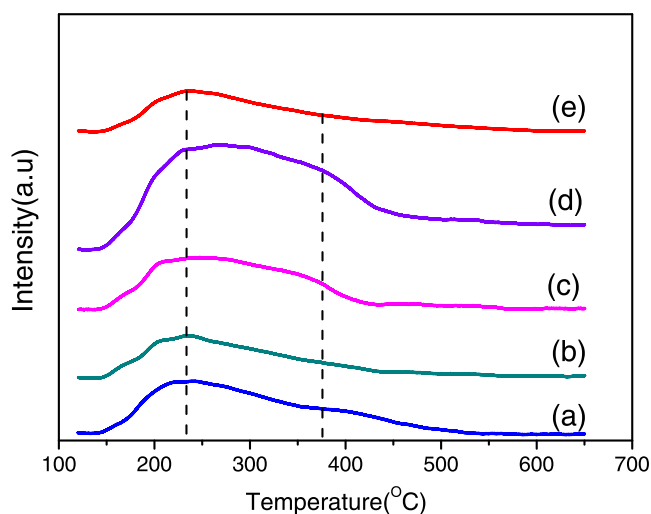

Figure 1. XRD patterns of the catalysts: (a) 30Ni5Cu/Al_2O_3, (b) 30Ni5Cu/Al_2O_3–SiO_2,(c) 30Ni5Cu/Al_2O_3–ZnO, (d) 30Ni5Cu/Al_2O_3–MgO, and (e) 30Ni5Cu/Al_2O_3–La_2O_3.
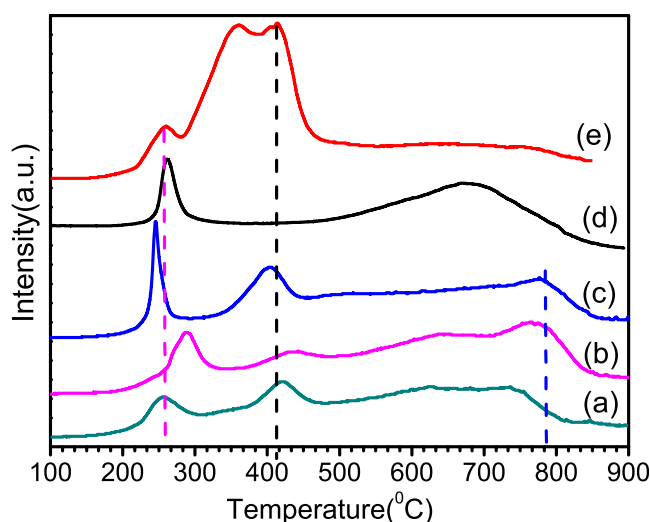
Figure 2. H_2-TPR profiles of the catalysts: (a) 30Ni5Cu/Al_2O_3, (b) 30Ni5Cu/Al_2O_3–SiO_2, (c) 30Ni5Cu/Al_2O_3–ZnO, (d) 30Ni5Cu/Al_2O_3–MgO, and (e) 30Ni5Cu/Al_2O_3–La_2O_3.

peak decreased, and the low-temperature reduction peak shifted to a higher temperature, which indicated that the introduction of SiO_2 can promote the dispersion of metal particles. For the 30Ni5Cu/Al_2O_3–ZnO catalyst, the low-temperature reduction peak shifted to a lower temperature and was significantly stronger than the high-temperature reduction peak, which infers that most of the NiO species on the catalyst occurred in a well-dispersed form.[23] For the 30Ni5Cu/Al_2O_3–MgO catalyst, only the low-temperature reduction peak was present in a significant intensity, indicating that almost all of the metal species on the support were uniformly dispersed. Three reduction peaks were observed for the 30Ni5Cu/Al_2O_3–La_2O_3 catalyst with a significantly higher proportion in the intensity of the high-temperature reduction peak, which was split into two peaks. This can probably be attributed to the separation of NiO and CuO because of agglomeration, suggesting that active metals were not dispersed well on the Al_2O_3–La_2O_3 carrier.

2.3. NH_3-Temperature-Programmed Desorption. NH_3-TPD curves of the catalysts in Figure 3 show that the

Figure 3. NH$_3$-TPD of the catalysts: (a) 30Ni5Cu/Al$_2$O$_3$, (b) 30Ni5Cu/Al$_2$O$_3$–SiO$_2$, (c) 30Ni5Cu/Al$_2$O$_3$–ZnO, (d) 30Ni5Cu/Al$_2$O$_3$–MgO, and (e) 30Ni5Cu/Al$_2$O$_3$–La$_2$O$_3$.

type of carrier has great effects on the adsorption of the reactants. For all of the catalysts, the desorption curves showed a gentle decline after the desorption peak temperature of about 230 °C. The shape of the desorption curves was very similar for 30Ni5Cu/Al$_2$O$_3$–ZnO and 30Ni5Cu/Al$_2$O$_3$–MgO, and the desorption peaks tailed to relatively high temperatures, nearly 400 °C. Combined with the analysis of the H$_2$-TPR curves, the active metals on the Al$_2$O$_3$–ZnO and Al$_2$O$_3$–MgO supports were mainly present as dispersed particles. These dispersed metal particles should provide the main active sites for adsorption and cause the desorption peak to extend to higher temperatures. For the catalysts 30Ni5Cu/Al$_2$O$_3$, 30Ni5Cu/Al$_2$O$_3$–SiO$_2$, and 30Ni5Cu/Al$_2$O$_3$–La$_2$O$_3$, desorption mainly occurred at relatively low temperatures, and no obvious trailing edge of the desorption peak was observed, which indicated that the active metal particles were mostly agglomerated and only provided weak adsorption for the reaction.

2.4. X-ray Photoelectron Spectroscopy. Table 1 shows the binding energies of the nuclear electrons bound to various

Table 1. Binding Energy of Core Electrons for Various Supports

support	binding energy (eV)				
	Al 2p	La 3d$_{5/2}$	Mg 2p	Zn 3d$_{3/2}$	Si 2p$_{3/2}$
Al$_2$O$_3$–MgO	74.08		49.83		
Al$_2$O$_3$–ZnO	74.56			1022.26	
Al$_2$O$_3$–La$_2$O$_3$	74.57	834.69			
Al$_2$O$_3$–SiO$_2$	74.57				102.95

active metal carriers. The AAl$_2$O$_3$–MgO carrier shows a Mg 2p XPS peak at 49.83 eV, which is similar to the results of other researchers for MgO (50.2 eV) or MgAl$_2$O$_4$ (50.2 eV). In the Zn 3d region of the XPS spectrum, Al$_2$O$_3$–ZnO exhibits a single peak of the Zn 3d$_{3/2}$ level at 1022.26 eV for ZnO or 1021.6–1022 eV for ZnAl$_2$O$_4$. In the Al$_2$O$_3$–La$_2$O$_3$ carrier, the La 3d5/2 signal with a binding energy of 834.69 eV is basically the same as the standard value of La$_2$O$_3$ (834.3 eV), which proves that La$_2$O$_3$ and Al$_2$O$_3$ have no force.

The chemical states of the elements Ni and Cu on the surfaces of various catalysts after reduction in H$_2$ at 650 °C were investigated by XPS, and the relevant information is shown in Table 2. The XPS spectra of all reduced catalysts contained the peak of Ni^0 (852.6 eV) and Ni^{2+} in nickel aluminate entities (856.2 eV). According to literature, the Cu 2p$_{3/2}$ lines appear at 932.4, 932.6, and 934.6 eV and are typically assigned to Cu$^+$, Cu^0, and Cu^{2+}. In the reduced catalyst samples, Cu species are identified as Cu^0 or Cu$^+$ species. On the surfaces of the Al$_2$O$_3$–ZnO and Al$_2$O$_3$–MgO carriers, the samples showed a relatively high Ni/Al ratio, while smaller Cu/Al ratios indicate the high dispersion of active species on these supports.[24] For 30Ni5Cu/Al$_2$O$_3$–SiO$_2$, 30Ni5Cu/Al$_2$O$_3$–La$_2$O$_3$, and 30Ni5Cu/Al$_2$O$_3$, the higher Cu/Al atomic ratio indicates that Cu caused a large amount of aggregation on the carrier surface.[25]

2.5. Catalytic Performance. 30NixCu/Al$_2$O$_3$ (x = 0, 5, 10, 15) catalysts were assessed for the production of hydrogen from ethanol from 400 to 600 °C at a molar H$_2$O/ethanol ratio of 4.0 and a GHSV of 8.0 h^{-1} Figure 4 compares the selectivities for products including H$_2$, CO, CH$_4$, and CO$_2$ over 30NixCu/Al$_2$O$_3$ (x = 0, 5, 10, 15) catalysts. Over the catalyst 30Ni0Cu/Al$_2$O$_3$, the selectivities for H$_2$, CO, CH$_4$, and CO$_2$ were 58.7, 33.4, 39.0, and 18.8% at 400 °C, respectively. The selectivity for H$_2$ and CO$_2$ increased while that for CH$_4$ decreased with temperature. CO selectivity exhibited a minimum of 9.4% at 450 °C, and the selectivities for H$_2$, CO, CH$_4$, and CO$_2$ were 90.0, 24.1, 7.4, and 58.8%, respectively, at a temperature of 600 °C. The 30Ni5Cu/Al$_2$O$_3$ catalyst showed the highest selectivity for H$_2$ and CO$_2$ in the temperature range of 400–600 °C, i.e., the selectivity for H$_2$, CO, CH$_4$, and CO$_2$ of 61.2, 29.6, 42.7, and 26.3% at 400 °C changed to 92.0, 32.3, 7.2, and 59.9% at 600 °C. When the Cu content was increased to 10 or 15 wt %, the selectivity for H$_2$ and CO$_2$ decreased in comparison to 30Ni5Cu/Al$_2$O$_3$–SiO$_2$ at the investigated temperatures, implying that the rates of the ethanol steam reforming reaction (C$_2$H$_5$OH + 3H$_2$O → 6H$_2$ + 2CO$_2$) and the WGS reaction (CO + H$_2$O → CO$_2$ + H$_2$) decreased when the Cu concentration was high.

Based on the established optimal catalyst composition of 30Ni5Cu/Al$_2$O$_3$, the performance of different composite supports for hydrogen production from ethanol was compared. Figure 5 shows the selectivity of various metal catalysts for H$_2$ from 400 to 600 °C. The catalysts with the composite supports Al$_2$O$_3$–MgO and Al$_2$O$_3$–ZnO demonstrated higher H$_2$ selectivity than other composite supports. The difference in H$_2$ selectivity of these metal catalysts becomes insignificant after the temperature reaches 600 °C.

For the 30Ni5Cu/Al$_2$O$_3$–MgO and 30Ni5Cu/Al$_2$O$_3$–ZnO catalysts, the effect of reaction temperature was further studied. Figure 6 shows the experimental results for 30Ni5Cu/Al$_2$O$_3$–MgO. When the temperature was lower than 300 °C, acetaldehyde was produced in the system due to the low conversion rate of ethanol conversion. When the temperature was increased from 300 to 600 °C, ethanol was completely converted, and thus, no ethylene and acetaldehyde were found in the system. These results show that Al$_2$O$_3$ supports containing MgO do not possess sufficient acidic sites for ethanol dehydration.[26] This Al$_2$O$_3$–MgO-supported catalyst was catalyzed by the following mechanisms: (i) dehydrogenation reaction on Cu sites and (ii) C–C bond breaking of acetaldehyde, formed as an intermediate product by the

Table 2. Binding Energies of Ni $2p_{3/2}$ and Cu $2p_{3/2}$ and Atomic Ratios on the Catalyst Surfaces

| samples	Ni $2p_{3/2}$ (eV)	Ni species	ratio (mol %)	Cu $2p_{3/2}$ (eV)	Cu species	ratio (mol %)	Ni/Al[a]	Cu/Al[b]
$30Ni5Cu/Al_2O_3$	852.6	Ni^0	49.19	932.7	$Cu^{0,+1}$	100%	0.29	0.094
	855.7	Ni^{2+}	50.81					
$30Ni5Cu/Al_2O_3-MgO$	852.5	Ni^0	55.6	932.6	$Cu^{0,+1}$	100%	0.61	0.067
	855.9	Ni^{2+}	44.4					
$30Ni5Cu/Al_2O_3-ZnO$	852.2	Ni^0	60.6	932.6	$Cu^{0,+1}$	100%	0.67	0.049
	855.8	Ni^{2+}	39.4					
$30Ni5Cu/Al_2O_3-La_2O_3$	852.3	Ni^0	41.6	932.3	$Cu^{0,+1}$	100%	0.20	0.13
	855.7	Ni^{2+}	58.4					
$30Ni5Cu/Al_2O_3-SiO_2$	852.6	Ni^0	67.6	932.5	$Cu^{0,+1}$	100%	0.34	0.12
	856.1	Ni^2	32.4					

[a]Nominal value: 0.59. [b]Nominal value: 0.09.
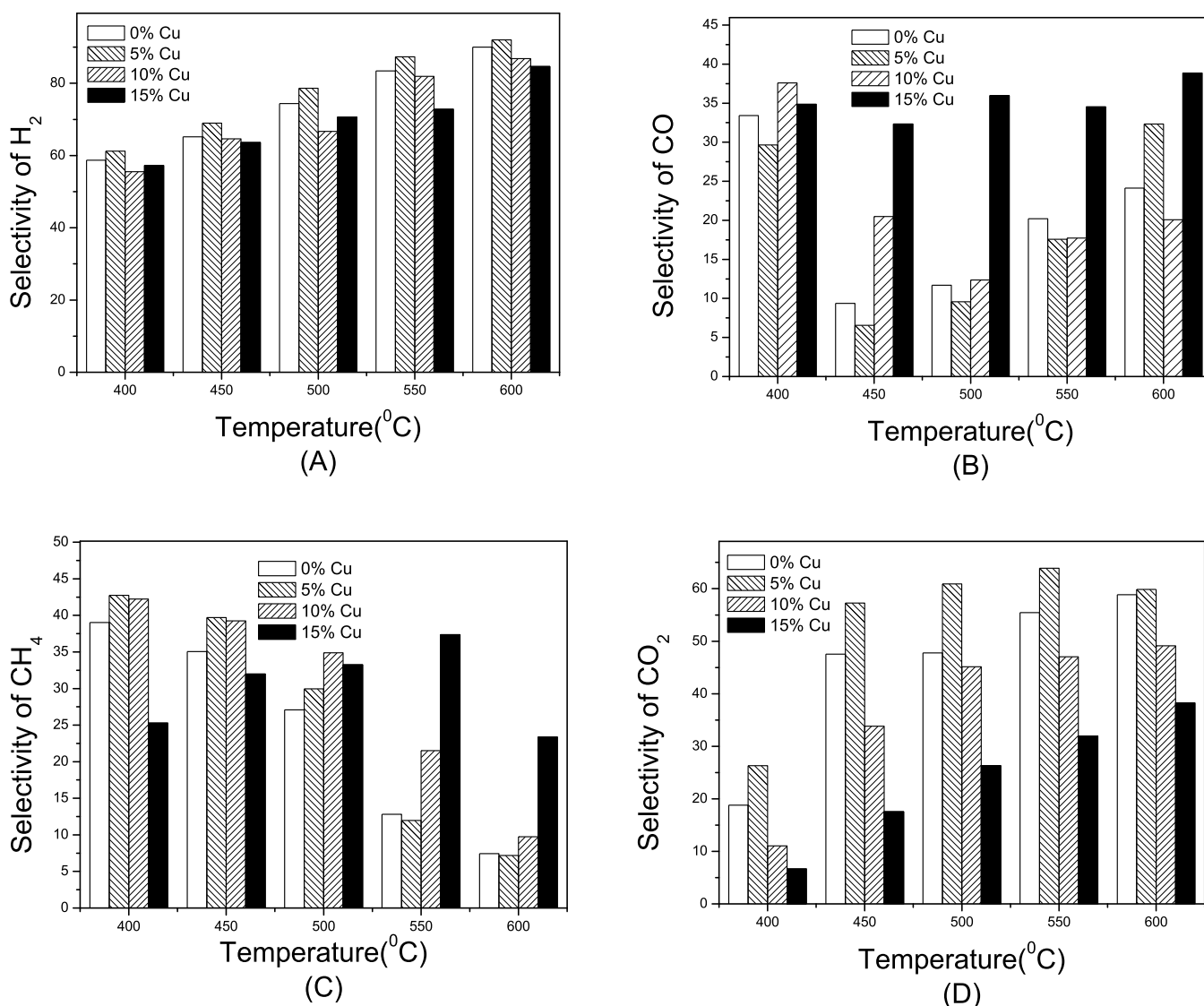
Figure 4. Effect of copper content on the $30NixCu/Al_2O_3$ catalyst performance for hydrogen production from ethanol reforming: (A) H_2 selectivity, (B) CO selectivity, (C) CH_4 selectivity, and (D) CO_2 selectivity.

dehydrogenation reaction, and generation of CO and CH_4 on the Ni site.[27]

As shown in Figure 6, H_2 selectivity increases with temperature. The selectivity to H_2 increased from 52.6% at 300 °C to 94.0% at 600 °C, indicating that the catalytic system has better selectivity to H_2. As the temperature increased from

300 to 600 °C, the water conversions were 10.7% (300 °C), 40.1% (450 °C), and 55.0% (600 °C). At the same time, the selectivity of CO and CO_2 also increases with the increase of temperature in the range of 300−600 °C. Meanwhile, the selectivity of the catalytic system to CH_4 reaches a maximum value as the temperature increases and then decreases to 11.0%
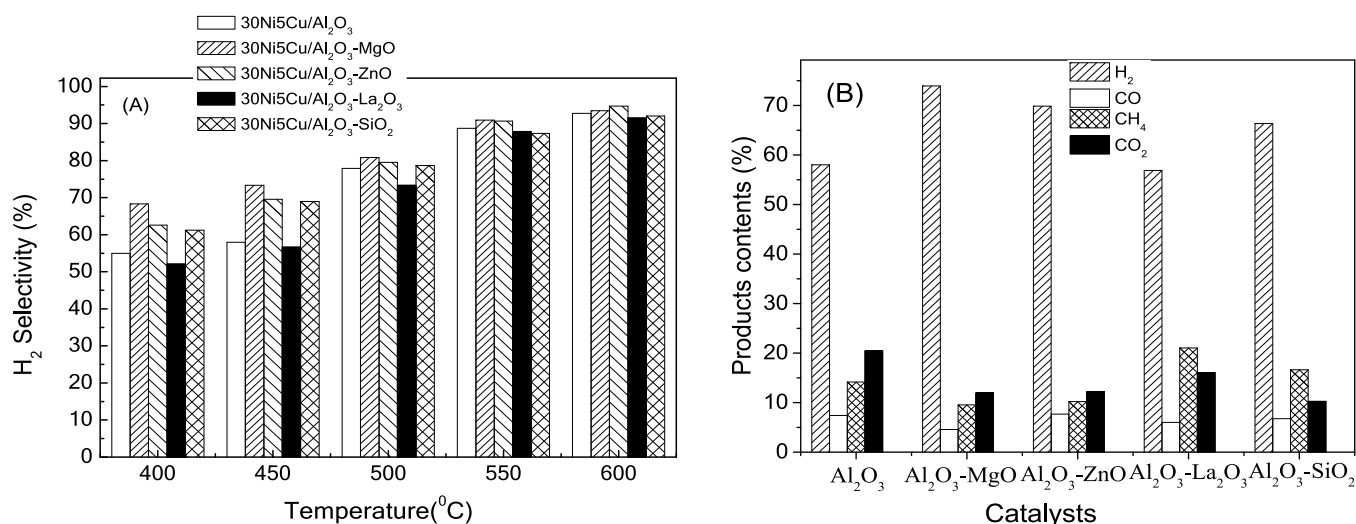
Figure 5. (A) H$_2$ selectivity in the investigated temperature range over different catalysts. (B) Product selectivities over different catalysts at 400–600 °C.
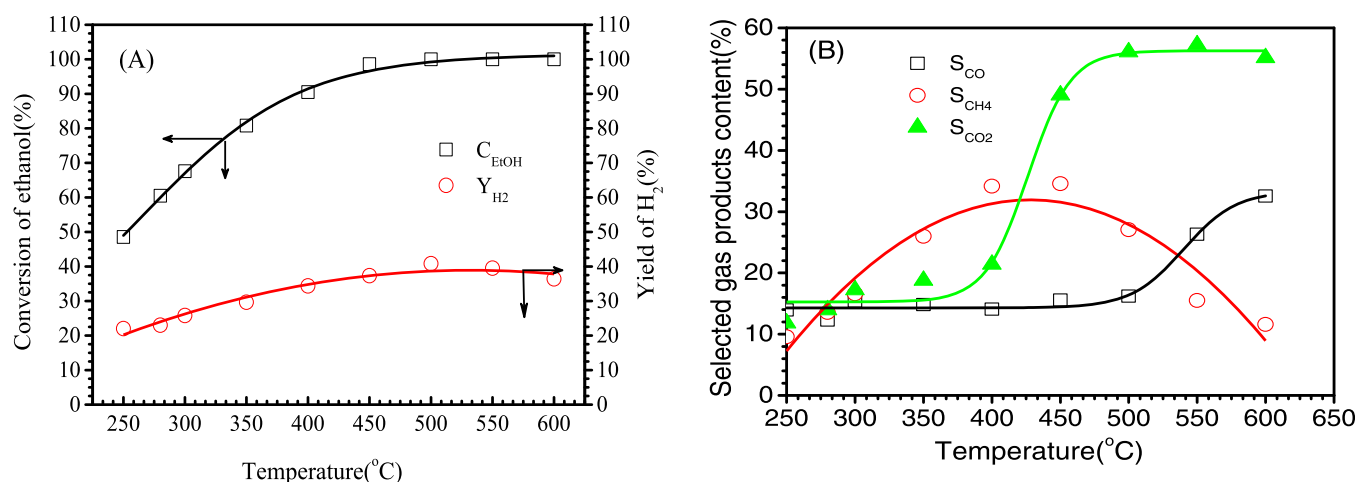
Figure 6. (A) Reactant conversion and yield of H$_2$ and (B) yield of other compounds on the 30Ni5Cu/Al$_2$O$_3$–MgO catalyst in ethanol steam reforming.
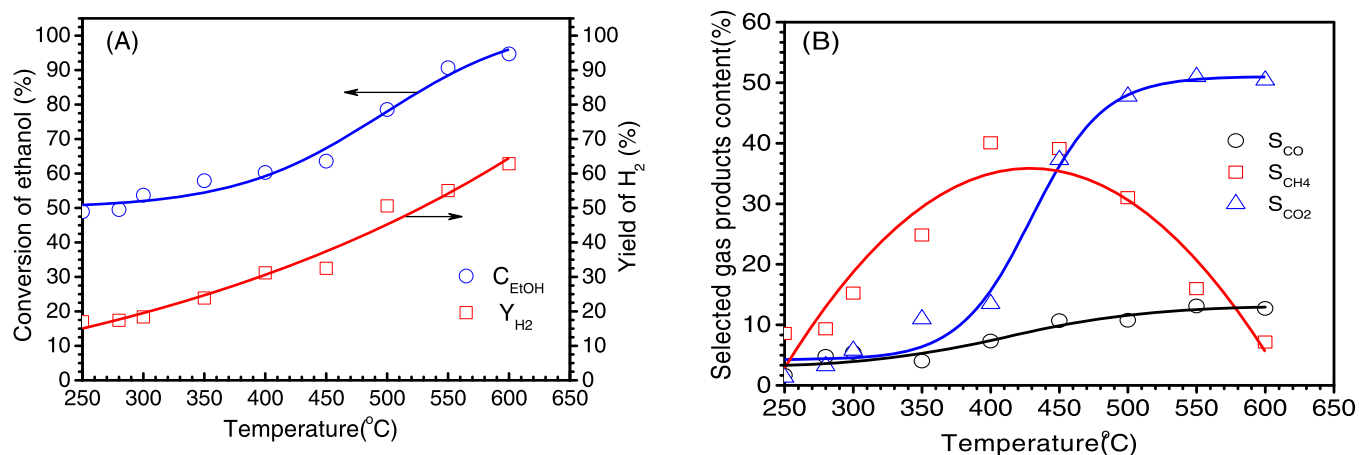
Figure 7. (A) Reactant conversion and yield of H$_2$ and (B) yield of other compounds on the 30Ni5Cu/Al$_2$O$_3$–ZnO catalyst in ethanol steam reforming.

as the temperature increases to 600 °C. It is shown that the reforming and reverse shift reactions of CH$_4$ are accelerated at the same time at elevated temperatures.

Figure 7 shows the catalytic effect of the catalyst with ZnO on the production of hydrogen from ethanol. We can know that as the temperature increases, ethanol is completely

converted, while acetaldehyde is only present at temperatures below 350 °C. At the same time, no ethylene was found in the whole testing process, indicating that $30Ni5Cu/Al_2O_3-ZnO$ greatly reduced the possibility of ethanol dehydration to ethylene due to its weak acidity.[28] As shown in Figure 7, H_2 selectivity increased with temperature. When the temperature was increased to 450 °C, the conversion of water was 32.5%, and the selectivities for H_2, CO_2, and CH_4 were 63.6, 37.5, and 39.1%, respectively. The results also indicate that the WGS reaction occurs and causes a decrease in CO selectivity. When the temperature increased to 600 °C, H_2 selectivity was 95.2%, while CH_4 selectivity was below 7.2%, and CO_2 selectivity increased to 63.3%; meanwhile, the selectivity to CO increased to 33.3%. These results suggest that CH_4 reforming and the reverse shift reaction were accelerated, while the WGS reaction gradually decreased.[29]

2.6. Thermogravimetric Analysis and Differential Scanning Calorimetry. In the process of ethanol reforming, ethanol dehydration probably occurred and produced ethylene, which was easily decomposed on the catalyst surface to form coke ($C_2H_4 \rightarrow 2C + 2H_2$).[30,31] To investigate the anticoking performance of the catalysts, TG and DSC experiments were conducted. Before the test, the $30Ni5Cu/Al_2O_3$, $30Ni5Cu/Al_2O_3-MgO$, and $30Ni5Cu/Al_2O_3-ZnO$ catalysts were catalyzed in the range of 250−600 °C at a temperature interval of every 50 °C for 2 h in the production of hydrogen from ethanol. Figure 8 shows the TG curves of the reacted
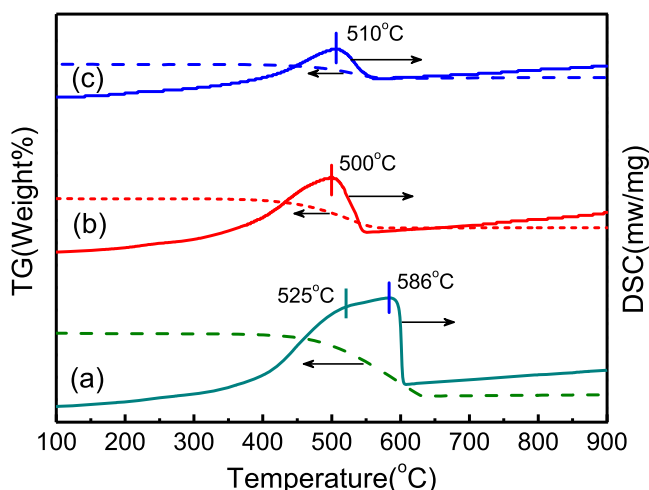
Figure 8. TGA and DSC profiles of (a) $30Ni5Cu/Al_2O_3$, (b) $30Ni5Cu/Al_2O_3-ZnO$, and (c) $30Ni5Cu/Al_2O_3-MgO$ catalysts.

catalyst to evaluate the moderate coking effect during the reaction. According to previous studies,[32,33] three forms of carbon are typically deposited on the catalyst during ethanol reforming, which are monoatomic carbon, filamentous coke, and graphitized carbon. But monoatomic carbon and filamentary coke can be easily removed by oxidation due to their high reactivity. However, as with increasing deposition of these two forms of carbon in catalytic systems, the possibility of graphitization of carbon is greatly increased. On the other hand, the formed graphitized carbon requires a higher temperature than the other two carbon species to react with O_2.[34] Therefore, we can know from the TGA curve that the peak below 550 °C is the oxidation of monoatomic carbon or filamentary coke in the catalytic system, while the higher

temperature peaks are attributed to the oxidation of graphitized coke in the catalytic system. Such graphitic carbon would greatly reduce the catalytic activity of this supported catalyst.[35] As calculated from the TG data, about 53% of the deposited coke present in $30Ni5Cu/Al_2O_3$ is graphite coke and a portion is other carbon coke. The monoatomic carbon and filamentary coke of $30Ni5Cu/Al_2O_3-MgO$ and $30Ni5Cu/Al_2O_3-ZnO$ account for most of them, so the proportion of graphite coke was below 10%. The supports of Al_2O_3-MgO and Al_2O_3-ZnO greatly decreased the formation of coke in the catalytic system, which was probably that the active metals are well dispersed on the support, so the catalyst has stronger adsorption performance.[36,37]

3. CONCLUSIONS

Catalysts loaded with two metals (Ni and Cu) on Al_2O_3 and $Al_2O_3-M_yO_z$ supports were prepared and their catalytic performances in the production of hydrogen from ethanol were investigated. The experimental results show that among these bimetallic supported catalysts, Cu, the one loaded with 5 wt %, has the best catalytic performance.

We prepared Ni−Cu-based bimetallic catalysts supported on $Al_2O_3-M_yO_z$ (M = Si, La, Mg, or Zn) based on a Cu content of 5 wt % and investigated the catalytic activity of the composite support on reforming of ethanol to hydrogen. Among them, Al_2O_3-MgO- and Al_2O_3-ZnO-supported catalysts demonstrated better catalytic activity than those supported on other research supports because of their better selectivity for H_2. For $30Ni5Cu/Al_2O_3-MgO$ and $30Ni5Cu/Al_2O_3-ZnO$, H_2 selectivities were 73.3 and 63.6% at 450 °C and increased to 94.0 and 95.2%, respectively, when the temperature was increased to 600 °C. Furthermore, the two catalysts exhibited much lower coking amounts and could probably be used as promising catalysts for hydrogen production by ethanol steam reforming.

4. EXPERIMENTAL SECTION

4.1. Catalyst Preparation. $Al_2O_3-M_yO_z$ carriers (M = La, Mg, or Zn) were prepared by a precipitation−impregnation method using a commercial γ-Al_2O_3 (Dow Chemicals, S_{BET} = 180 m^2/g) powder, and the molar ratio of M/Al in mixed oxide was fixed at 0.25. A 0.1 M aqueous urea solution was dropped into a 0.1 M aqueous solution of lanthanum(III) nitrate, magnesium(II) nitrate, or zinc(II) nitrate and mixed well at 100 °C with constant stirring.

Then, γ-Al_2O_3 powder was added to the above solution, and stirring was continued at 100 °C for 6 h. The mixture was filtered and the resulting solid was dried at 120 °C and then calcined in air at 650 °C for 6 h. The mixed solid was ground and sieved to obtain the catalyst carriers with a size of 0.2−0.3 mm. They were labeled $Al_2O_3-M_yO_z$, where M refers to the metal element (Mg, Zn, and La) of the second oxide. In a typical experiment, $Al_2O_3-SiO_2$ supports were prepared by the sol−gel method. First, $Al(NO_3)_3\cdot9H_2O$ was dissolved in distilled water, and the pH of the solution was adjusted to 3.0−3.5 with dilute nitric acid, and a stoichiometric amount of tetraethoxysilane (TEOS) (SiO_2/Al_2O_3 molar ratio of 0.25) was added to 0.347 g/mL $Al(NO_3)_3$. After mixing for 5 h, the pH of the solution was adjusted to 3.0 to obtain a floc, which was finally adjusted with dilute nitric acid.

Ni and Ni−Cu catalysts were synthesized by a precipitation−impregnation method using the prepared $Al_2O_3-SiO_2$,

Al_2O_3−MgO, Al_2O_3−ZnO, and Al_2O_3−La_2O_3 supports as well as the commercial γ-Al_2O_3 support. The nominal Ni loadings on the supports were fixed at 30 wt %. Stoichiometric amounts of an aqueous nickel(II) nitrate solution (0.1 M) and an aqueous copper(II) nitrate solution (0.1 M) were added to the supports, and then, aqueous urea solution (0.1 M) was added at 100 °C. The suspension was filtered, and the obtained solid was dried at 120 °C and calcined in air at 650 °C for 6 h. This supported metal catalyst was designated $30NixCu/Al_2O_3$−M_yO_z (x = 0, 5, 10, 15, M = Mg, Zn, La, and Si), where the catalyst $30Ni5Cu/Al_2O_3$−MgO is represented as an Al_2O_3−MgO carrier containing 30 wt % Ni and 5 wt % Cu.

4.2. Catalyst Characterization. The crystals of the materials were analyzed by X-ray diffraction (XD-3 diffractometer, Beijing Purkinje General Instrument Co., Ltd., China). The instrument used Cu Kα radiation (λ = 0.15418 nm) and was operated at 40 kV and 40 mA. XRD patterns were collected at 2θ angles from 5 to 85°. X-ray photoelectron spectroscopy (XPS) was conducted with a Kratos Axis Ultra DLD spectrometer with a Mg Kα X-ray source. The reduction temperature of different supported metal catalysts was investigated using H_2-TPR and NH_3-TPD Micromeritics AutoChem 2920 V3.05 instruments. Specifically, H_2-TPR was used at a heating rate of 10 °C/min from room temperature to 900 °C. The NH_3-TPD experiments were carried out by heating samples to 650 °C at a heating rate of 10 °C/min at a He flow rate of 50 mL/min while using a thermal conductivity detector (TCD) to determine the NH_3 concentration in the system.

4.3. Activity Tests. The experiments for the production of hydrogen from ethanol reformation were conducted in a stainless steel tubular reactor (inner diameter = 12 mm, length = 360 mm) operating at atmospheric pressure. The catalyst (150 mg) was diluted in a volume ratio of 3:1 using SiC (0.2−0.3 mm) per experiment to avoid unfavorable thermal reactions. After placement of the diluted supported catalyst, the reactor was purged with N_2 at 200 °C and then reduced with H_2 (30 mL (STP)/min) at 650 °C for 40 min at a heating rate of 10 °C/min. After the pretreatment gas was removed by flushing the reactor with N_2, a mixture of water and ethanol at a molar ratio of 4.0 was fed into the evaporator at a rate of 1.2 mL/h by a syringe pump, and then, a mass flow controller was used with the N_2 mix supplied at a flow rate of 80 mL/min. After gasification at 150 °C, the reaction products were analyzed by online GC-TCD (chromatograph model 3420, Agilent) using a Porapak Q packed column (id = 2 mm, length = 5.0 m, CO_2, ethane, ethylene, water, acetaldehyde, ethanol, acetone, acetic acid, diethyl ether, ethyl acetate, and crotonaldehyde) and a TDX-01 packed column (id = 2 mm, length = 3.0 m, H_2, N_2, CO, CH_4, CO_2, and ethylene) in series with He as the carrier gas. Ethanol conversion denoted as $X_{ethanol}$, H_2 selectivity denoted as S_{H_2}, and the selectivity to carbon products denoted as $S_{icarbon}$ are evaluated according to the following equations

$$X_{ethanol} = \frac{F_{ethanol-in} - F_{ethanol-out}}{F_{ethanol-in}} \quad (1)$$

$$S_{H_2} = \frac{F_{gas}V_{H_2}}{6(F_{ethanol-in} - F_{ethanol-out})} \quad (2)$$

$$S_{icarbon-containing\ product} = \frac{F_{icarbon-containing\ product}}{n(F_{ethanol-in} - F_{ethanol-out})} \quad (3)$$

where $F_{ethanol}$ is the molar flow rate of ethanol, F_{gas} is the total gas flow rate, V_{H_2} is the volume content of H_2 in the gas products, and n denotes the ratio of the calculated number of carbon atoms in ethanol to the number of carbon atoms in the product.

■ AUTHOR INFORMATION

Corresponding Authors

Hongjun Zhou − *College of Chemistry and Chemical Engineering, Zhongkai University of Agricultural and Engineering, Guangzhou 510225, China;* ⓘ orcid.org/0000-0002-4210-6327; Phone: 86-20-89003114; Email: hongjunzhou@163.com

Zhenyu Jia − *College of Chemistry and Chemical Engineering, Zhongkai University of Agricultural and Engineering, Guangzhou 510225, China;* Phone: 86-20-89002608; Email: gdjiazhenyu@163.com

Author

Qihai Liu − *College of Chemistry and Chemical Engineering, Zhongkai University of Agricultural and Engineering, Guangzhou 510225, China*

Complete contact information is available at:
https://pubs.acs.org/10.1021/acsomega.1c06579

Notes

The authors declare no competing financial interest.

■ REFERENCES

(1) Özkan, G.; Şahbudak, B.; Özkan, G. Effect of molar ratio of water/ethanol on hydrogen selectivity in catalytic production of hydrogen using steam reforming of ethanol. *Int. J. Hydrogen Energy* **2019**, *44*, 9823−9829.

(2) Chen, D.; Liu, C. L.; Mao, Y. Y.; Wang, W. J.; Li, T. L. Efficient hydrogen production from ethanol steam reforming over layer-controlled graphene-encapsulated Ni catalysts. *J. Cleaner Prod.* **2019**, *252*, No. 119807.

(3) Khani, Y.; Bahadoran, F.; Soltanali, S.; Ahari, J. S. Hydrogen production by methanol steam reforming on a cordierite monolith reactor coated with Cu−Ni/LaZnAlO₄ and Cu−Ni/γ-Al₂O₃ catalysts. *Res. Chem. Intermed.* **2018**, *44*, 925−942.

(4) Goula, M. A.; Sotiria, K. K.; Panagiotis, E. T. Hydrogen production by ethanol steam reforming over a commercial Pd/γ-Al2O3 catalyst. *Appl. Catal., B* **2004**, *49*, 135−144.

(5) Menegazzo, F.; Cristina, P.; Danny, Z.; Michela, S.; Cas, B.; Guido, D. M.; Alessandro, Z. Hydrogen Production by Ethanol Steam Reforming on Ni-Based Catalysts: Effect of the Support and of CaO and Au Doping. *ChemistrySelect* **2017**, *2*, 9523−9531.

(6) Vizcaíno, A. J.; Carrero, A.; Calles, J. A. Hydrogen production by ethanol steam reforming over Cu−Ni supported catalysts. *Int. J. Hydrogen Energy* **2007**, *32*, 1450−1461.

(7) Bruno, J. E.; Dwarica, N. S.; Whittaker, T. N.; Hand, T. N.; Guzman, C. S., IV; Dasgupta, A.; Chen, Z. F.; Rioux, R. M.; Chandler, B. D. Supported Ni−Au Colloid Precursors for Active.; Selective.; and Stable Alkyne Partial Hydrogenation Catalysts. *ACS Catal.* **2020**, *10*, 2565−2580.

(8) Luo, S.; Song, H.; Philo, D.; Oshikiri, M.; Kako, T.; Ye, J. H. Solar-driven production of hydrogen and acetaldehyde from ethanol on Ni−Cu bimetallic catalysts with solar-to-fuels conversion efficiency up to 3.8%. *Appl. Catal., B* **2020**, *272*, No. 118965.

(9) Wu, Y. F.; Gui, W. Y.; Liu, X. F.; Zhang, L.; Wang, S. X.; Wang, Z. L.; Zhang, C. L. Promotional Effect of Cu for Catalytic Amination of Diethylene Glycol with Tertiarybutylamine over Ni−Cu/Al$_2$O$_3$ Catalysts. *Catal. Lett.* **2020**, *150*, 2427−2436.

(10) Parlett, C. M. A.; Durndell, L. J.; Isaacs, M. A.; Liu, X. T.; Wu, C. F. Ethanol Steam Reforming for Hydrogen Production Over Hierarchical Macroporous Mesoporous SBA-15 Supported Nickel Nanoparticles. *Top. Catal.* **2020**, *63*, 403−412.

(11) Miao, C. X.; Zhou, G. L.; Chen, S.; Xie, H. M.; Zhang, X. M. Synergistic effects between Cu and Ni species in NiCu/γ-Al2O3 catalysts for hydrodeoxygenation of methyl laurate. *Renewable Energy* **2020**, *153*, 1439−1454.

(12) de Andrade, T. S.; Souza, M. M. V. M.; Manfro, R. L. Hydrogenolysis of glycerol to 1.; 2-propanediol without external H$_2$ addition in alkaline medium using Ni−Cu catalysts supported on Y zeolite. *Renewable Energy* **2020**, *160*, 919−930.

(13) Shejale, A. D.; Yadav, G. D. Noble metal promoted Ni−Cu/ La$_2$O$_3$-MgO catalyst for renewable and enhanced hydrogen production via steam reforming of bio-based n-butanol: effect of promotion with Pt.; Ru and Pd on catalytic activity and selectivity. *Clean Technol. Environ. Policy* **2019**, *21*, 1323−1339.

(14) Xie, Z. B.; Chen, B. F.; Wu, H. R.; Liu, M. Y.; Liu, H. Z.; Zhang, J. L.; Yang, G. Y.; Han, B. X. Highly efficient hydrogenation of levulinic acid into 2-methyltetrahydrofuran over Ni−Cu/Al$_2$O$_3$-ZrO$_2$ bifunctional catalysts. *Green Chem.* **2019**, *21*, 606−613.

(15) Xue, H. Y.; Gong, X. X.; Xu, J. J.; Hu, R. R. Performance of a Ni−Cu-Co/Al$_2$O$_3$ Catalyst on in-situ Hydrodeoxygenation of Bio-derived Phenol. *Catalysts* **2019**, *9*, No. 952.

(16) Hu, N. M.; Yang, C. H.; He, L.; Guan, Q. Q.; Miao, R. R. Ni−Cu/Al$_2$O$_3$ catalysts for the selective hydrogenation of acetylene: a study on catalytic performance and reaction mechanism. *New J. Chem.* **2019**, *43*, 18120−18125.

(17) Sahu, C.; Khan, F.; Pandey, P. K.; Pandey, M. Study of Ni−Cu/Al$_2$O$_3$ Catalyst for Hydrodeoxygenation of Karanja Oil. *Asian J. Chem.* **2017**, *29*, 647−649.

(18) Seyedeh, M. M. N.; Seyed, M. A.; Golshan, M. Modeling and optimization of methane dry reforming over Ni−Cu/Al$_2$O$_3$ catalyst using Box-Behnken design. *J. Energy Chem.* **2018**, *27*, 219−232.

(19) Rategarpanah, A.; Meshkani, F.; Wang, Y.; Arandiyan, H.; Rezaei, M. Thermocatalytic conversion of methane to highly pure hydrogen over Ni−Cu/MgO•Al$_2$O$_3$ catalysts: Influence of noble metals (Pt and Pd) on the catalytic activity and stability. *Energy Convers. Manage.* **2018**, *166*, 268−280.

(20) Charisiou, N. D.; Italiano, C.; Pino, L.; Sebastian, V.; Vita, A.; Goula, M. A. Hydrogen production via steam reforming of glycerol over Rh/γ-Al$_2$O$_3$ catalysts modified with CeO$_2$.; MgO or La$_2$O$_3$. *Renewable Energy* **2020**, *162*, 908−925.

(21) Wang, Y.; Chen, M.; Yang, Z.; Liang, T.; Liu, S.; Zhou, Z.; Li, X. Bimetallic Ni-M (M = Co.; Cu and Zn) supported on attapulgite as catalysts for hydrogen production from glycerol steam reforming. *Appl. Catal., A* **2018**, *550*, 214−227.

(22) Dou, B.; Zhang, H.; Cui, G.; He, M.; Ruan, C.; Wang, Z.; Chen, H.; Xu, Y.; Jiang, B.; Wu, C. Hydrogen sorption and desorption behaviors of Mg-Ni−Cu doped carbon nanotubes at high temperature. *Energy* **2019**, *167*, 1097−1106.

(23) Sun, Y.; Xiong, C.; Liu, Q.; Zhang, J.; Tang, X.; Zeng, X.; Liu, S.; Lin, L. Catalytic Transfer Hydrogenolysis/Hydrogenation of Biomass-Derived 5-Formyloxymethylfurfural to 2.; 5-Dimethylfuran Over Ni−Cu Bimetallic Catalyst with Formic Acid As a Hydrogen Donor. *Ind. Eng. Chem. Res.* **2019**, *58*, 5414−5422.

(24) Ibrahim, S.; Cheng, Y.; Zhao, D.; Nadeem, M. A. A new insight for photocatalytic hydrogen production by a Cu/Ni based cyanide bridged polymer as a co-catalyst on titania support in glycerol water mixture. *Int. J. Hydrogen Energy* **2019**, *44*, 2508−2518.

(25) Muñoz-Batista, M. J.; Motta Meira, D.; Colón, G.; Kubacka, A.; Fernández-García, M. Phase-contact engineering in mono and bimetallic Cu-Ni co-catalysts for hydrogen photo-production materials. *Angew. Chem., Int. Ed.* **2018**, *57*, 1119−1203.

(26) Cross, A.; Miller, J. T.; Danghyan, V.; Mukasyan, A. S.; Wolf, E. E. Highly Active and Stable Ni−Cu Supported Catalysts prepared by Combustion Synthesis for Hydrogen Production from Ethanol. *Appl. Catal., A* **2018**, *572*, 124−133.

(27) Liang, T.; Wang, Y.; Chen, M.; Yang, Z.; Liu, S.; Zhou, Z.; Li, X. Steam reforming of phenol-ethanol to produce hydrogen over bimetallic Ni Cu catalysts supported on sepiolite. *Int. J. Hydrogen Energy* **2017**, *42*, 28233−28246.

(28) Yang, X.; Fu, X.; Bu, N.; Han, L.; Wang, J.; Song, C.; Su, Y.; Zhou, L.; Tiao, L. Promotion effect of nickel for Cu−Ni/γ-Al$_2$O$_3$ catalysts in the transfer dehydrogenation of primary aliphatic alcohols. *J. Iran. Chem. Soc.* **2017**, *14*, 111−119.

(29) Alves Da Silva, F.; Pontes, I. D.; Wurzler, G. T.; Alonso, C. G.; Neto, A. M.; Scaliante, M. H. N. O.; DeSouza, M.; Fernandes-Machado, N. R. C. Production of hydrogen from bioethanol in Cu−Ni/NbxOy catalysts obtained by different preparation methods. *Int. J. Hydrogen Energy* **2016**, *41*, 8111−8119.

(30) Bedia, J.; Barrionuevo, R.; Rodriguez-Mirasol, J.; Cordero, T. Ethanol dehydration to ethylene on acid carbon catalysts. *Appl. Catal., B* **2011**, *103*, 302−310.

(31) Chen, B. H.; Lu, J. Z.; Wu, L. P.; Chao, Z. S. Dehydration of bio-ethanol to ethylene over iron exchanged HZSM-5. *Chin. J. Catal.* **2016**, *37*, 1941−1948.

(32) Vicente, J.; Montero, C.; Erena, J.; Azkoiti, M. J.; Bilbao, J.; Gayubo, A. G. Coke deactivation of Ni and Co catalysts in ethanol steam reforming at mild temperatures in a fluidized bed reactor. *Int. J. Hydrogen Energy* **2014**, *39*, 12586−12596.

(33) Wu, C. F.; Williams, P. T. Investigation of coke formation on Ni-Mg-Al catalyst for hydrogen production from the catalytic steam pyrolysis-gasification of polypropylene. *Appl. Catal., B* **2010**, *96*, 198−207.

(34) Nolan, P. E.; Schabel, M. J.; Lynch, D. C.; Cutler, A. H. Hydrogen control of carbon deposit morphology. *Carbon* **1995**, *33*, 79−85.

(35) Obregón, I.; Gandarias, I.; Miletić, N.; Ocio, A.; Arias, P. L. One-Pot 2-Methyltetrahydrofuran Production from Levulinic Acid in Green Solvents Using Ni−Cu/Al$_2$O$_3$ Catalysts. *ChemSusChem* **2015**, *8*, 3483−3488.

(36) Saeki, T.; Ohkita, H.; Kakuta, N.; Mizushima, T. Synergistic effects of CeO2-supported bimetallic Ni−Cu, Co−Cu, and Ni−Fe catalysts on steam reforming of ethanol. *J. Ceram. Soc. Jpn.* **2015**, *123*, 955−960.

(37) Miao, C.; Zhou, G.; Chen, S.; Xie, H.; Zhang, X. Synergistic effects between Cu and Ni species in NiCu/γ-Al$_2$O$_3$ catalysts for hydrodeoxygenation of methyl laurate. *Renewable Energy* **2020**, *153*, 1439−1454.